

A New Technique for Visualizing Microboiling Phenomena and its Application to Water Pulse-Heated by a Thin Metal Film

C. Thomas Avedisian¹, Richard E. Cavicchi², Michael J. Tarlov²

¹Sibley School of Mechanical and Aerospace Engineering
Cornell University
Ithaca, New York 14853-7501

²Process Sensing Group
Chemical Science and Technology Laboratory
National Institute of Standards and Technology
Gaithersburg, Maryland 20899

ABSTRACT

This paper presents a laser strobe microscopy method for photographing fast transient microscale processes. The technique is illustrated by capturing time-lapsed images of bubble nucleation from pulse-heated thin films immersed in a pool of water. The method combines a pulsed laser for the light source and a microscope with 100X magnification of a heater element (platinum film, 30 microns long, 15 microns wide, and 0.2 microns thick immersed in water), and associated instrumentation to coordinate the laser pulse with the electrical pulse at various delay times to step through the evolutionary process of the phase change. The emphasis of this paper is on describing the experimental method and illustrating its capabilities to record the nucleation and growth of microbubbles.

Results show bubble nucleation and morphology in subcooled water for electrical (heating) pulses with duration ranging between 0.50 μs to 1 μs . The repeatability of the process, which is an essential requirement for obtaining meaningful information on the evolution of the phase change process, is demonstrated which allows high effective framing

rates to be achieved ($> 10^8 \text{ s}^{-1}$) using a pulsed light source with a controlled delay. New bubble morphologies are shown. For $0.5 \mu\text{s}$ pulses bubbles appear to nucleate first at the corners of the heater followed by lateral coalescence and spreading to form a thin vapor film which later thickens on the heater footprint and evolves into an oblate spheroidal shape. For $1 \mu\text{s}$ pulses, individual bubbles are observed which appear at specific nucleation 'sites' that may indicate surface imperfections typical of nucleate boiling processes even though the superheat is close to the superheat limit of water.

INTRODUCTION

The ability to photographically document processes that occur on small length and time scales (i.e., micro/nano) is becoming increasingly important to gaining an understanding of a number of industrially important problems. Bubble nucleation and growth as related to ink jet printing technology is one such process. It is initiated by a programmed voltage to a thin metal film immersed in the ink (typically water-based) which resistively heats the film and forms the bubble at conditions close to the spontaneous nucleation temperature of the liquid [1]. The subsequent rapid expansion of the bubble forces the ejection of liquid from a nozzle aligned with the heater, thus forming print characters when the heater is moved in a programmed way. Bubble formation and growth near the spontaneous nucleation limit is characterized by extremely high heating rates ($\sim 10^8$ °C/s), as for the case of water heated close to 300°C [2]. At such heating rates bubble nucleation, once initiated, is predicted to be a faster process than growth of trapped vapor or gas nuclei at an equivalent temperature [3]. The important process in this application is the dynamics of growth and collapse of the bubble which occurs on such a small length (micrometer) and time (microsecond) scale that conventional means for imaging which do have the requisite time resolution [4] are difficult or impossible to apply due to their physical size.

There are additional applications in which bubble nucleation on small length and/or time scales plays a key role, and for which application of imaging capabilities which can resolve the relevant scales of the process would benefit the understanding of the underlying mechanisms. For example, the inkjet process is being explored for use in applications outside of printing on paper. Examples include fabrication of polymer electronics and printed circuit boards [5], DNA arrays [6-8], deposition of cells [9], combinatorial studies of materials synthesis [10,11], pharmaceutical studies [12]. Micromachined fuel injectors [13] using an inkjet-like process have also been reported. Applications in microfluidics where bubble nucleation figures prominently include bubble-

pumps and mixers [14]. Another application is the imaging of living cells maintained far from equilibrium that can spontaneously form chemical and concentration patterns [15]. All of these applications are highly dynamic and require the ability to image on the microscale with a micro or nano-second time resolution.

In this paper we describe our method for photographing a microscale time-dependent event with nanosecond resolution, and demonstrate its capabilities for the problem of bubble nucleation and growth associated with pulse heating a thin film heater in water - the process relevant to thermal ink jet printing as described above. A pulsed light source is coupled with electronic triggering to image bubble dynamics through a microscope fitted with a high magnification water immersion lens and a digital camera for image capture. Water at room temperature is the working fluid.

While a complete description of the phase change process will couple visualization of bubble morphology with measurement of the average surface temperature (which is the signature variable that defines the nucleation mechanism (i.e., homogeneous or heterogeneous)), we focus in this paper on the visualization aspect of the problem only, and not on the method to record the average surface temperature under pulse heating conditions. Measurements of the average surface temperature of pulse-heated thin film heaters immersed in subcooled liquids have been presented in earlier publications [2,16].

Existing techniques to record fast transient processes capture the entire history of a single event through either exposing film that is mechanically drawn past the shutter, or by employing etched photoelectric detectors in a two-dimensional array distributed around the lens and then sequentially triggered to record the process at an effective frame speed dictated by the time at which the detector is triggered. The fastest such cameras commercially available appear to operate at a frame rate of $2 \times 10^8 \text{ s}^{-1}$ [4] for a time step of 5 ns. The relatively high expense of these systems limits their wider use. Furthermore, because CCD technology is used, the spatial resolution of the resultant images do not yet match that of film.

When the physical scale of the bubble nucleation and growth process is of order micrometers in size, photography through a microscope is required. Skripov [17] first used a Xenon flash lamp as the light source for recording microboiling associated with pulse-heating 10 μ m diameter platinum wires in various fluids where the lamp was triggered off the voltage pulse to the heater; this approach was later used by Glod et al [18] where the flash duration was 500ns. These studies have shown that in some instances bubble growth can occur on a time frame that challenges the ability of flash illumination to "freeze" the image to allow recording fine features of the process. Shorter duration light flashes are required.

The approach described here is applicable to processes that have a sufficiently high degree of repeatability that time-lapsed photography can be used to construct the evolutionary behavior of the event. Fast-transient microboiling is such an event. A series of images of the event are obtained using a light flash of sufficiently short duration to minimize image blurring. By systematically varying the delay time of the flash for acquiring the images, they can be viewed sequentially to obtain the evolution of the process. The "framing rate" in this approach is dictated by both the duration of the light flash, and the temporal precision of each image as dictated by the 'jitter' of the flash. The idea of taking images at different delay times can be traced to the earliest days of flash photography [19]. More recently, it has formed the basis of recording the dynamics of droplet impingement at a solid surface using a simple arrangement that couples a flash lamp with a 35 mm camera and appropriate delay circuitry [20,21]. Movies created in this fashion have a time resolution that surpasses that of commercial imaging systems and at a much lower cost. This is achieved through the flexibility of using either film to capture the image or a digital camera with appropriate resolution (e.g., 6x10⁶ pixels being about the limit for a print of A4 size). It should be noted that gated imaging methods where the light source is constant (and can be of much longer duration) but the acquisition of the image takes place via a pulsed imaging diode or microchannel plate are also possible [22], but may have drawbacks of cost, resolution, and ease of implementation.

The use of a laser as a very short flash for microscale imaging has been reported for studies of laser-induced bubble nucleation on melanosomes [23,24]. These tests are inherently non-repeatable so for each delay between nucleation and imaging, a different melanosome must be characterized. Stasicki et al. [25] report a laser flash study on IR-laser induced liquid microjet disintegration, in which a series of images was collected by imaging successive jet events with different delay times. Recently, our experimental apparatus was used by Balss et al. [26,27] to record bubble nucleation for surfaces with conditioned wetting by self-assembled monolayers. This capability allowed for the first time to resolve details with nanosecond resolution of bubble morphology during the phase transition process that characterizes some of the applications mentioned previously (e.g., thermal ink jet technology). A variation of this theme discussed here later employed a laser diode for illumination to provide 30ns temporal resolution [28].

In the next sections, we discuss the experimental arrangement and present results for bubble nucleation of water at atmospheric pressure to illustrate the capabilities. While some of the physics of this process are illustrated and discussed, the emphasis of the paper is on the hardware description and a demonstration of its capabilities for a fast transient microscale process.

EXPERIMENTAL APPARATUS

We are interested in bubble nucleation that is triggered by a heat (voltage) pulse of duration (τ) ranging from 0.5 μ s to 5 μ s while the heating element is immersed in a fluid, here being water. During this time, a light source triggered at a particular instant exposes a photographic element (film or CCD) during the pulse. For each heating event, one picture is taken which corresponds to the trigger time. The time sequence is then constructed by progressively delaying the trigger time. The duration of the light source dictates image clarity.

The goal of microphotography as applied in our study is to record a time-varying image with minimal image blurring, here being of the rapid growth and collapse of a bubble on a

pulse-heated thin film. Taking $\dot{R} (\equiv dR/dt)$ as the bubble growth rate and Δ as the physical distance that is acceptable for the object to move while a photographic element is exposed, then a pulsed light source with $\frac{\Delta}{\dot{R}}$ as the pulse duration is necessary to ensure image clarity.

In the experiment, the microscope can resolve dimensions of about 0.5 μm , and a typical bubble growth rate is on the order of 30 m/s [27]. Thus, the duration of the light flash should be about 17 ns or less to give the illusion of 'freezing' an event of this scale moving at this speed. Here, we use the illumination provided by a Nd:Yag laser with a measured flash duration (FWHM) of 7.5 ns. Other laser technologies with shorter pulse durations than used here are also applicable.

The main elements of the experimental apparatus are the following: pulsed laser light source with appropriate hardware for beam conditioning; personal computer (PC) for controlling the time sequence; microscope for image magnification; digital camera; power supply for heating the element; electronic instrumentation for coordinating power to the heater with delay and activation of the laser; and thin film heater.

Figure 1 is a schematic diagram that illustrates the major components of the arrangement, which are the following: pulse light source (Q-switched Nd:Yag laser, Surelite II [29] with the 1064nm line frequency doubled to produce a 532nm beam (the color of all images is green)); Nikon Labophot II to which was attached a 100X objective water-immersion lens (Olympus LUMPlanF1, 100X/1.00W, $\infty/0$ objective lens); Nikon D100 digital camera (with 6×10^6 pixel resolution) for image capture; SRS DG535 digital-gate-and-delay generator for coordinating the Q-switch, and camera shutter activation; HP 8116A function generator for triggering an electrical pulse to the heater element; bridge circuit to facilitate measuring the change of voltage associated with electrically heating the thin film; Agilent 8411a pulse generator for delivering a programmed voltage to the bridge circuit that heats the platinum film; and a PC running a LabVIEW program to automate triggering of the pulse generator that heats the thin film; digital oscilloscope (LeCroy LT354) to observe and record the waveform of the voltage

output from the bridge circuit and to aid in balancing the bridge in real time prior to the start of an experiment.

The 532 nm beam was split using a half-wave plate and polarizing beam splitter. The majority of the beam energy was dumped into a beam trap, and the remainder was directed into a multimode fiber patch cable (Thorlabs, Inc, #M21L01) terminated with a collimator lens (Thorlabs, Inc., #F220SMA-A) at the fiber input side. At the fiber output, the beam was imaged into the universal illumination port of the microscope through a 25 mm focal length plano-convex lens. Because of the high laser power, the internal lenses of the microscope illumination port were replaced by coated lenses that could withstand the laser power without cracking. Neutral density filters (optical density = 0.7) attenuated the laser power so as not to burn the optics or heat the platinum film. The latter effect was noted as a potential concern in measurements of surface temperature (not reported here) when no neutral density filters were used. We tested a variety of fiber optic cables with different diameters and found that the one selected provided the highest quality light for microphotography. Indeed, the image quality was found to be very sensitive to the illumination intensity, laser beam path to the microscope, and fiber optic. For example, with too much light to the camera images would appear bright and bleached of color with poor contrast. We note that the fiber optic cable and collimator are rated by the supplier for much lower laser powers. As a result, the collimator and fiber optic cable were periodically replaced due to damage from the high intensity laser, which manifested itself in the form of clouding the collimator lens by ionizing gases and adhesive that was burned by the laser.

The heater element was a platinum thin film 0.2 μm thick, 15 μm wide and 30 μm long. Limited observations of bubble nucleation are included for a 100 μm long heater. This physical size was selected so that its entire area was in the field of view of the 100X lens. As previously noted, using low aspect-ratio (length/width) heaters comes at the expense of inducing temperature gradients along the imaged area during a heat pulse, as compared to

high aspect-ratio (~ 50) heaters as used in previous work (e.g., Thomas et al. [16]) where temperature gradients are negligible. This effect is expected to be more pronounced for platinum compared to a higher thermal conductivity material (e.g., aluminum). As will be observed in the next section, bubble nucleation was evident at selected locations.

A LabVIEW program was written to direct electrical signals to the DG535 which set the delay for triggering the Q-switch for successive pulses and nucleation events triggered the Agilent 8411a pulse generator to power the heater and produce a bubble. Prior to triggering the Q-switch, the camera shutter was open for 0.5 s, then closed for 0.5 s and the process repeated at a rate of 1 Hz. The camera aperture was set manually throughout the experiments. The ASA (American Standards Association) number was selected to optimize image quality for each set of operating conditions and ranged between 800 and 1600 for the photographs reported here. Images were stored in the camera's memory card after taking a series of photographs and then downloaded to the PC and viewed with Nikon Image Capture V3.0 software.

The sequence of events for the various operations is illustrated in figure 2. The delay to trigger the laser, t_d , is set at the gate and delay generator. Images are taken at $t_d=(n-1)\Delta t$ where Δt is the programmed time step for the flash and $n=1,2,3,\dots$ for images 1, 2, 3, respectively in the series of photographs. In our experiments we used time steps between photographs in the range $2 \text{ ns} \leq \Delta t \leq 100 \text{ ns}$. Note that the flash lamp is triggered well before the Q-switch, thus giving the lasing medium sufficient time to be pumped by the flashlamp. As recommended by the manufacturer the laser Q-switch delay was set to 180 ms with respect to the flash lamp trigger. t_g is the pulse generator delay which is manually adjusted to position the electrical pulse (duration τ) so that the flash is triggered within the time window of the electrical pulse to the heater. Once set, it is not changed. Similarly, the time at which a bubble nucleates, t_b , is controlled by the input voltage pulse to the bridge (V_{in}) and τ .

To present the operational performance of the photomicroscopy method described here, we generally tried to adjust parameters so that bubble nucleation occurred at halfway to two-thirds of the pulse duration as shown in the schematic of figure 2. Examples of actual bridge voltage outputs are illustrated in figures 3 and 4 for the conditions given in the caption. The heater response is shown in terms of voltage output from the bridge circuit rather than surface temperature (which would be obtained by a separate calibration) because the variable of interest here - inflection point temperature - is well described in this raw data format. The significance of the inflection point temperature in terms of the physics of homogeneous nucleation has been discussed previously in which it was shown that inflection point voltages illustrated in figures 3 and 4 are close to 300C for water [2,16]. The input voltage that produced the output response in figures 3 and 4 shows an inflection point that is about 2/3 of the total pulse width. The pulse width (τ) in figure 3 was 1.0 μ s and for figure 4 it was 5.0 μ s.

Figures 3 and 4 show that the inflection point becomes much less pronounced as τ decreases. For $\tau \sim 0.5 \mu$ s we could not observe a clear inflection point to signify bubble nucleation, as the output signal exhibited significant noise due to the high frequency of the on/off cycle at these values of τ . Nonetheless, our photographs clearly showed the presence of bubbles (discussed in the next section) even when the evolution of output voltage (surface temperature) did not indicate their presence from an inflection point. This illustrates the importance of high frequency photographic imaging as presented here, coupled with metrology for quantitative surface temperature measurement [2,16] to provide a suite of capabilities to analyze the rapid nucleation/growth/collapse process associated with bubble nucleation on pulse heated surfaces.

We did not rely on the nominal specification of the pulse duration of the laser provided by the manufacturer and instead measured it. The pulse time dictates both the effective framing rate and the time assigned to each of the captured images. The precise time at which the light is emitted from the laser was also found to be variable and exhibited some 'jitter'. The laser

pulse duration and jitter were measured with a photodetector (Thorlabs, Inc., #DET210) with a rise time of 1 ns coupled to the oscilloscope. Measurements of the average temporal profile of the laser pulse, triggered from the Q switch, were averaged from 4000 individual pulses with the results shown in figure 5. The temporal profile of the light intensity exhibits a nearly Gaussian form as evidenced by the Gaussian fit (solid line) to the data (symbols) in figure 5. The fit to the data in figure 3 yields a 'full width half maximum' for the laser pulse, t_{FWHM} , of 7.46 ns which represents the nominal pulse duration produced by the laser. A 'jitter' (t_j) on the peak can also be inferred from the averaged measurements in figure 5 and data from a single shot. For example, selecting an arbitrary individual pulse (which appears qualitatively like figure 5), we estimated $t_{FWHM,i} = 6.81$ ns. Defining t_j as

$$t_j \equiv \sqrt{|t_{FWHM}^2 - t_{FWHM,i}^2|} \quad 1$$

gives $t_j \approx 3.0$ ns. This means that the peak in figure 5 would occur with a nominal uncertainty of about this value which is also the uncertainty of the time assigned to each photograph. An alternative analysis would involve averaging each individual pulse history (with a form similar to that shown in figure 5) to determine t_j . However, the above estimate is appropriate for present purposes.

The framing rate is determined by the time step of the delay, Δt , as

$$FR = \frac{1}{\Delta t} \quad 2$$

It may be possible to obtain useful information when $\Delta t < t_{FWHM}$ using image analysis methods. But the presence of jitter sets an absolute limit on the maximum meaningful framing rate, FR_{max} , of $1/t_j$,

$$FR_{\max} \approx \frac{1}{t_j}$$

3

Attempting to collect data at a higher rate, $FR > FR_{\max}$ will result in blurred images. Based on our value for t_j , FR_{\max} is approximately 3.3×10^8 frames/s.

In the next section we present results for heater pulse durations of $0.5 \mu\text{s}$, $1.0 \mu\text{s}$ and $5 \mu\text{s}$. Recent studies examined heating pulses of $5 \mu\text{s}$ pulse as related to thermal ink jet processes and chemical detection [2,16,26,27]. We found that smaller pulse widths produced unique bubble morphologies that were also useful for demonstrating the capabilities of the apparatus described above. At the same time, the sharpness of the inflection point appears to diminish with τ as noted previously.

RESULTS

The images in all of our photographs were obtained by fixing the focal plane on the substrate. In this way, we could automate the flash microscopy arrangement in figure 1 where the LabVIEW program coordinates the voltage pulses that open the camera shutter, triggers the heating pulse and the laser Q-switch to expose the sensor element of the camera. In our procedure, pictures were taken (and the laser fired) at a frequency of 1 Hz. Automation of image capture facilitates acquiring many photographs at progressively later delays and, thus, at later stages of bubble growth. However, it comes at the expense of producing images that can have significant blurring when the bubble grows away from the focal plane (i.e., the substrate).

Figure 6 shows selected images of bubbles formed $3.8 \mu\text{s}$ after initiation of a $5 \mu\text{s}$ pulse, and figure 6b is a schematic illustrating the issue of image blurring. The 'dots' shown in the left side of figure 6a are bond pad 'vias'. The images in figure 6 are from two distinct nucleation events. For (b) the substrate is in focus and for (a) the bubble periphery is in

focus. It was possible to set the focal plane on the bubble periphery because the nucleation process could be made to appear quasi-steady and stationary when the laser and heating pulse frequencies were appropriately adjusted (indicative of the repeatability of the process). However, it is proved extremely time-consuming to re-focus each image on the bubble periphery (a). There are distinct advantages to substrate-focusing (b) because of the automation it allows for image capture, but blurring of the bubble boundary will influence the precision of the area-averaged diameter [27], D_{eq} , due to edge blurring as shown in (b). The precision of the area-averaged diameter value will have an uncertainty commensurate with the thickness of the diffuse interface boundary.

As noted previously, the validity of developing a time sequence from individual images rests on the repeatability of the process. Figure 7 shows measured effective bubble diameters determined from digital images of a bubble taken at precisely $3.8 \mu\text{s}$ after initiation of a voltage pulse to the thin film heater – the same delay time as for the images in figure 6. Area-averaged bubble diameter measurements were made using a computer-based image analysis package (ImagePro Plus software) in which the bubble boundary is user-defined based on a selected gray-scale value. The data are from 19 different nucleation events. The data in figure 7 show that there is remarkably close agreement of the diameters obtained from photographs in which the focal plane was the substrate (figure 6b) and bubble periphery (figure 6a). However, it should again be noted that it is virtually impossible to automate image capture to focus on the bubble periphery because the growth of the bubble into the bulk and away from the surface makes the focal plane of the periphery time dependent. Nonetheless, if care is taken to choose the grayscale of the image in the image analysis program, the error in obtaining dimensions from blurred images (e.g., those shown in figure 6a(i)) can be small.

Figure 8 shows a series of photographs illustrating a complete time sequence of bubble growth and collapse for a $0.5 \mu\text{s}$ pulse. The nucleation process occurs between 0 and $0.05 \mu\text{s}$. Four bubbles appear at the corners of the heater ($0.10 \mu\text{s}$) and the bubble evolves into a film

that is flat to the heater ($0.20 \mu\text{s}$). The film then begins to grow into the bulk ($0.45 \mu\text{s}$) after which the bubble periphery becomes progressively blurred signifying growth away from the substrate. The bubble continues to grow well after the termination of the $0.5 \mu\text{s}$ pulse, and eventually starts to collapse as the bubble condenses ($2.35 \mu\text{s}$ to $3.6 \mu\text{s}$).

The complete growth/collapse cycle in figure 8 spans the order of the pulse width, τ . However, we can resolve times much shorter than τ by changing the trigger delay time to obtain greater resolution and detail of the bubble growth process. This is shown in figure 9 where times between 58 ns and 246 ns are isolated to illustrate greater time resolution in figure 8 between $0.55 \mu\text{s}$ and $2.7 \mu\text{s}$. As further shown in figure 9 nucleation starts by bubbles forming at the corners of the heater (58 ns), probably indicating the existence of a nonuniform surface temperature. Within the central region of the heater, a cluster of smaller bubbles then become visible that seem to indicate the presence of multiple nucleation sites as shown at 86 ns . These bubbles merge to form a sheet anchored at the corners almost like a liquid bridge (142 ns) which thickens (178 ns) as evidenced by the shadow on the periphery. At 246 ns the sheet covers almost the entire heater footprint after which the bubble grows perpendicular to the surface and the bubble periphery starts to become blurred.

The bubble morphology appears to be dependent on the pulse width, as the unusual nucleation process described above was only observed for $\tau \leq 1 \mu\text{s}$. At longer pulse widths [26,27], the initial nucleation event was not observed as four bubbles in the corners as shown in figure 9 (58 ns) but rather as isolated individual bubbles within the central region of the heater. This fact complicates explanation if a nonuniform surface temperature exists that makes the corners hotter, perhaps due to a nonuniform film thickness which is thinner at the corners than the central region. Further investigation is required to better understand the influence of parameters on the initial nucleation and growth process for particularly short pulse widths.

As a final point, we note again that the basis of developing time sequences such as shown in figures 8 and 9 is the pulse-to-pulse repeatability of the process. We found that virtually all bubble features shown in figures 8 and 9 were quite repeatable, as verified by fixing the trigger delay, taking a sequence of photos at that delay, and comparing. For example, for Figure 9 at 178 ns the photographs showed a remarkable repeatability right down to the ruffled edges of the liquid/vapor interface which indicate an instability to the growth process. Even the beginning of the process where the vapor sheet develops as shown between 86ns and 142 ns in figure 9 was repeatable. Figure 10 shows three photographs in a set where the delay was fixed at 107 ns after initiation of the trigger pulse which illustrates this repeatability.

CONCLUSIONS

We have described a method to photographically record details of the nucleation and growth process of vapor bubbles on thin film heaters that cover the smallest scales of length and time which are relevant to many industrial applications. Bubble nucleation is extremely repeatable even when triggered by a programmed voltage pulse of sub-microsecond duration. For a 0.5 μ s heater pulse duration, bubbles nucleate at the corner of the heater and grow to form a vapor sheet that remains in focus for a period that indicates that the sheet is flat to the substrate. Eventually, the sheet thickens, the periphery becomes progressively blurred and the bubble grows perpendicular to the surface. Bubble growth continues well after the voltage pulse to the heater is terminated, which indicates significant inertia in the process.

The maximum framing rate will be influenced by the parameters of the light source (flash duration and jitter), and the methodology described here is versatile enough to accommodate a variety of laser pulses and cameras for recording formats.

ACKNOWLEDGEMENTS

The authors are pleased to acknowledge the many discussions and contributions of Drs. Joseph Hodges, Cary Presser, Owen Thomas, Christopher Montgomery, Roger van Zee, John Suehle, Karin Balss, Lori Goldner and Wilbur Hurst.

REFERENCES

1. R.R. Allen, J.D. Meyer, W.R. Knight, *Hewlett Packard J.* 36, 21-27 (1985).
2. C. T. Avedisian, W. S. Osborne, F. D. McLeod, C. M. Curley, *Proc. R. Soc. Lond. A* 455, 3875-3899 (1999).
3. A. Asai, *J. Heat Trans.* 113, 973-979 (1991).
4. Smith, E., *Popular Science*, 72-78, 102, 104, July (2003).
5. J. Bharathan, Y. Yang, *App Physics Letters* 72, 2660-2662 (1998).
6. T. Goldmann, J. S. Gonzalez, *J. Biochem. Biophys. Methods* 42, 105-110 (2000).
7. A. Bietsch, M. Hegner, H. P. Lang, C. Gerber, *Langmuir* 20, 5119-5122 (2004).
8. P. J. Park et al., *J. Biotech.* 112, 225-245 (2004).
9. E. A. Roth et al., *Biomaterials* 25, 3707-3715 (2004); T. Xu, J. Jin, C. Gregory, J. J. Hickman, T. Boland, *Biomaterials* 26, 93-99 (2005).
10. H. M. Reichenbach, P. J. McGinn, *J. Mat. Res.* 16, 967-974 (2001); X. D. Sun et al., *Advanced Materials* 9, 1046-& (1997).
11. A. V. Lemmo, J. T. Fisher, H. M. Geysen, D. J. Rose, *Analytical Chemistry* 69, 543-551 (1997).
12. A. V. Lemmo, D. J. Rose, T. C. Tisone, *Current Opinion in Biotechnology* 9, 615-617 (1998).
13. M. Ching-Yi, Y. Jinn-Cherng, W. Chou-Lin, C. Ching-Long, C. Chun-Jung, *Final Program and Proceedings of IS&T's NIP19: International Conference on Digital Printing Technologies*, 338-342 (2003); M. Ching-Yi, Y. Jinn-Cherng, W. Chou-Lin, C. Ching-Long,

- C. Chun-Jung, Final Program and Proceedings of IS&T's NIP19: International Conference on Digital Printing Technologies, 294-297 (2003).
14. B. C. Khoo, E. Klaseboer, K. C. Hung, Sensors and Actuators a-Physical 118, 152-161 (2005); K. Okuyama, R. Takehara, Y. Iida, J. H. Kim, Microscale Thermophysical Engineering 9, 119-135 (2005).
 15. Petty, H.R. Optics & Photonics News, 15 (1), 40-45 (2004).
 16. Thomas, O. C., Cavicchi, R. E., Tarlov, M. J. Langmuir, 19 (15), 6168-6177 (2003).
 17. Skripov, S. Superheated Liquids, pp. 113, 169, 170, 171, Hemisphere Publishing Co. (1974).
 18. Glod, S.; Poulikakos, D., Zhao, Z., Yadigaroglu, G. J. Heat Mass Transf. 45, 367-379 (2002).
 19. Edgerton, H.E. 1979 Electronic Flash Strobe, 2nd Ed., Cambridge: The MIT Press.
 20. Chandra, S., and Avedisian, C.T., Proc. R. Soc. Lond., A432, 13-41 (1991).
 21. Chandra, S., and Avedisian, C.T., Int. J. Heat Mass Transf., 35, 2377-2388 (1992).
 22. Frank, A. M. and Wilkins, P. R. Proceedings of the SPIE, 4183, 170-6, (2001).
 23. Lin, C. P. and Kelly, M. W., Applied Physics Letters, 72, 2800-2802, (1998).
 24. Neumann, J. and Brinkmann, R., Proceedings of the SPIE, 4617, 180-185, Laser Tissue Interaction XIII: Photochemical, Photothermal, and Photomechanical; Steven L. Jacques, Donald D. Duncan, Sean J. Kirkpatrick, Andres Kriete; Eds. (2002).
 25. Stasicki, B., Charvat, A., Faubel, M. and Abel, B., Proceedings of the SPIE, 5580, 335-346, (2005).
 26. Balss, K.M., Thomas, O.C., Avedisian, C.T., Cavicchi, R.E. and Tarlov, M.J. 'Factors Influencing Microboiling Behavior on Gold Microheaters,' 226th National Meeting of the American Chemical Society, Division of Colloid and Surface Chemistry, New York, September 7-11 (2003).
 27. Balss, K.M., Avedisian, C.T., Cavicchi, R.E. and Tarlov, M.J. Langmuir, 21, 10459-10467, (2005).

28. Hong, Y., Ashgriz, N. and Andrews, J. ASME J. Heat Transfer. 126, 259-271 (2004).

Neumann, J. and Brinkmann, R. Proc. SPIE, Vol. 4617A, Laser Tissue Interaction XIII, 180-185 (2002).

29. Certain commercial instruments are identified to adequately specify the experimental procedure. In no case does such identification imply endorsement by the National Institute of Standards and Technology. This statement applies to all instruments mentioned in this paper.

Figure Captions

Figure 1: Schematic of micro-imaging system for recording bubble growth under pulse heating conditions.

Figure 2: Schematic of trigger sequence for heating the thin film and pulsing the laser.

Figure 3: Output voltage for a 1 μs pulse at $V_{\text{in}} = 15.4\text{V}$. Inflection point signifies bubble nucleation.

Figure 4: Output voltage for a 5 μs pulse at $V_{\text{in}} = 4.49\text{V}$. Inflection point signifies bubble nucleation.

Figure 5: Temporal profile of the light intensity (arbitrary units) from Surelite II laser. Each point in time is an average of 4000 laser pulses. The solid line is a least-squares Gaussian fit to the data.

Figure 6: Illustration of focal planes on bubble image. Photographs taken 3.8 μs after initiation of a 5 μs heating pulse: (a) focus on bubble periphery (substrate is blurred). Photographs are from two different heat pulses taken at the same delay time; (b) focus on substrate (bubble perimeter is blurred).

Figure 7: Effective bubble diameter obtained from images where the substrate is in focus ($D_{\text{eq-s}}$) and the bubble periphery is in focus ($D_{\text{eq-b}}$). Bubble images are 3.8 microseconds after a 5 μs pulse; figure 4 shows representative images of the two focal planes.

Figure 8: Evolution of bubble morphology in time increments of 50 ns (effective framing rate of 20 million frames/s); nucleation is triggered by an input voltage to the platinum film of 11.8V over a time of 0.5 μ s.

Figure 9: Photographs showing more detail of the evolution of bubble morphology in the early period of nucleation and growth for $\tau = 0.50 \mu$ s, $V_{in}=11.8V$, and $\delta t = 2$ ns. Time beneath each image is relative to the first appearance of the bubbles. The bubbles are visible at the four corners of the platinum film at 58 ns and coalesce to form a sheet that covers the surface by 142 ns. At 86 ns, the interior of the sheet is populated by clusters of microbubbles which eventually coalesce into a film at 178 ns.

Figure 10: Images of different pulse heating events illustrating repeatability, taken 0.107 μ s after start of a 0.5 μ s pulse.

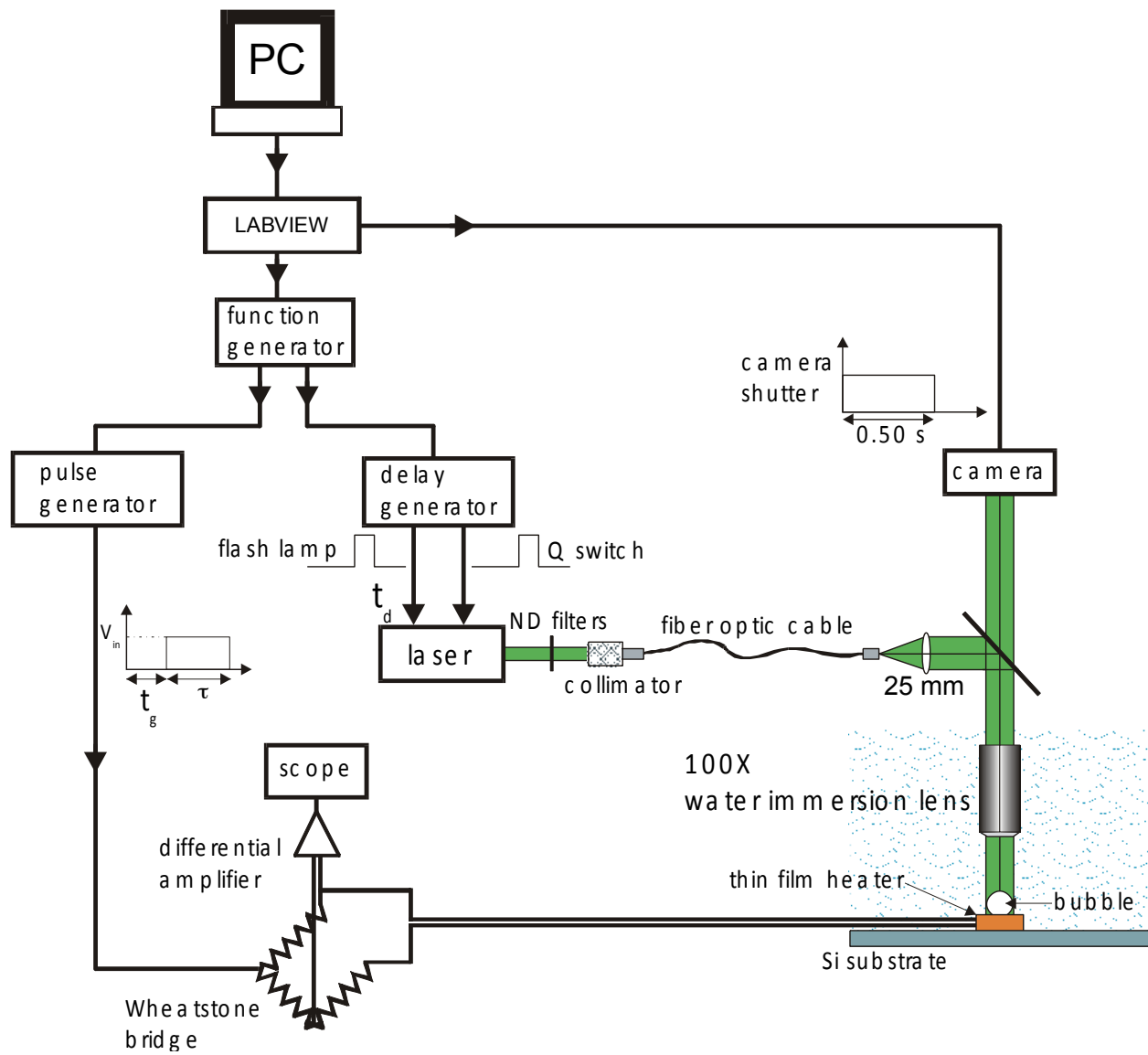


Figure 1

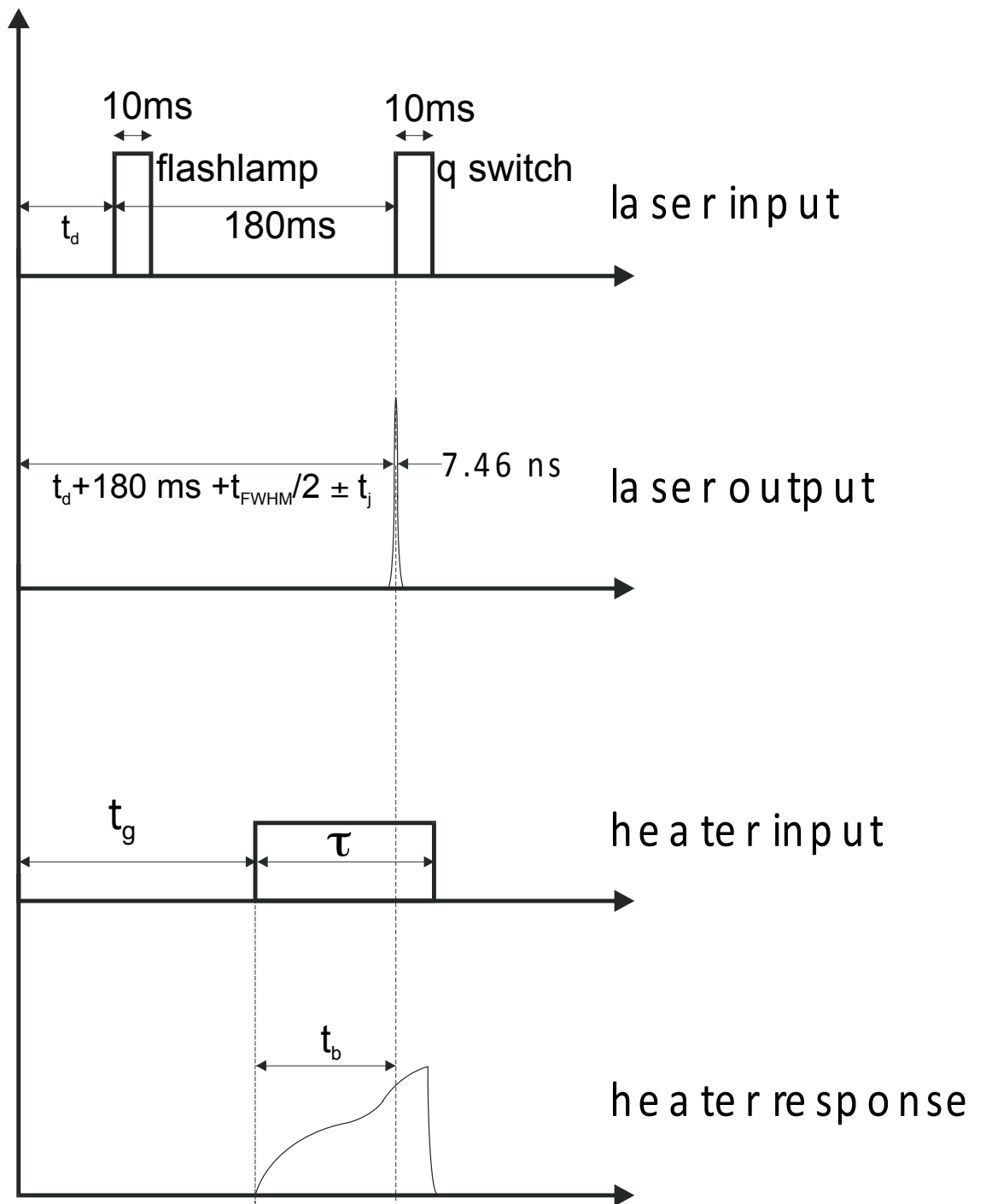


Figure 2

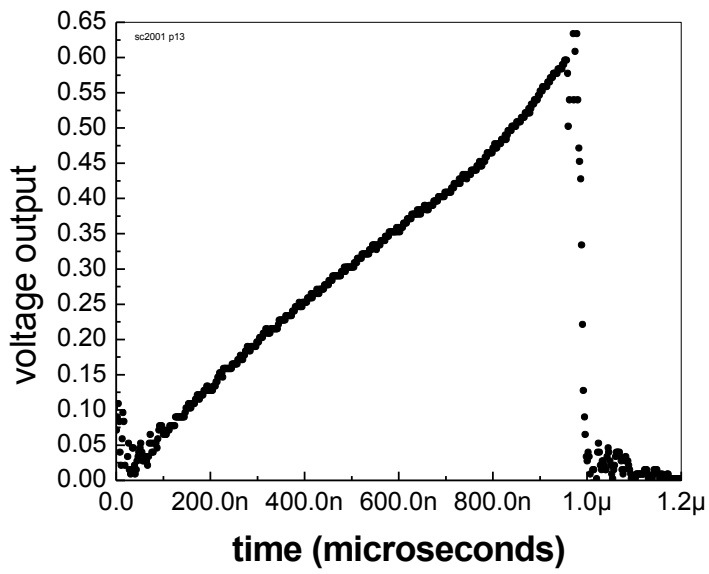


Figure 3

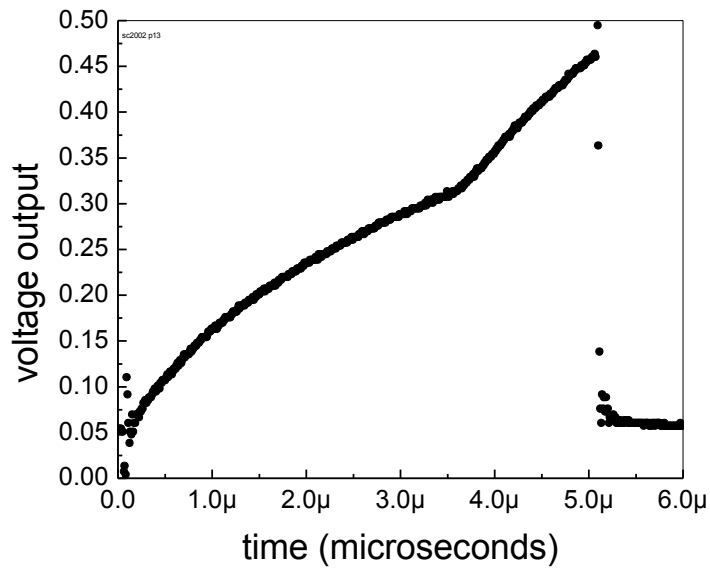


Figure 4

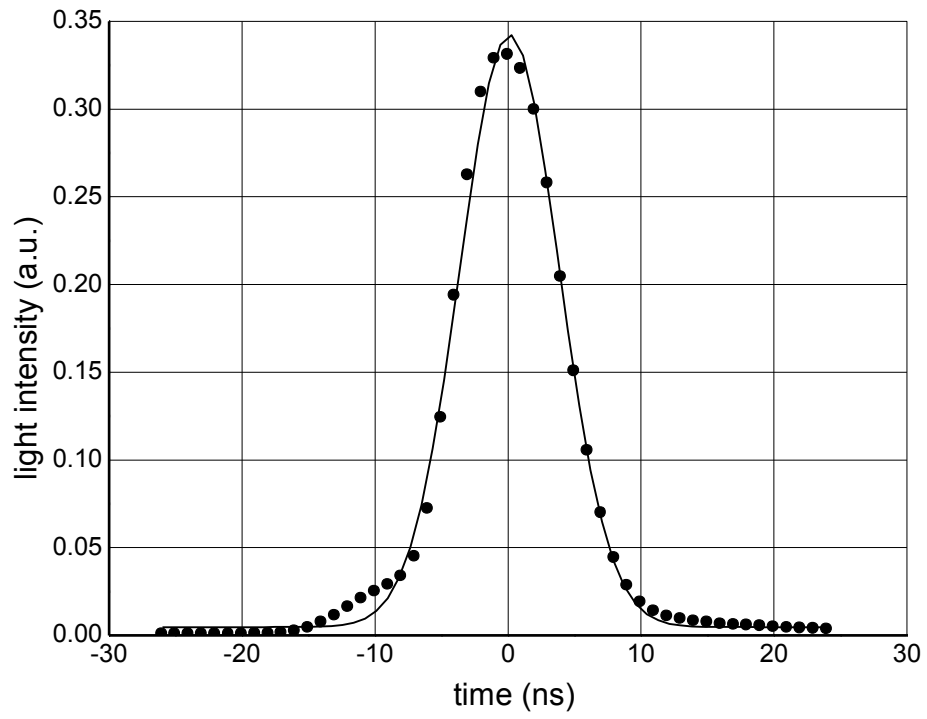


Figure 5

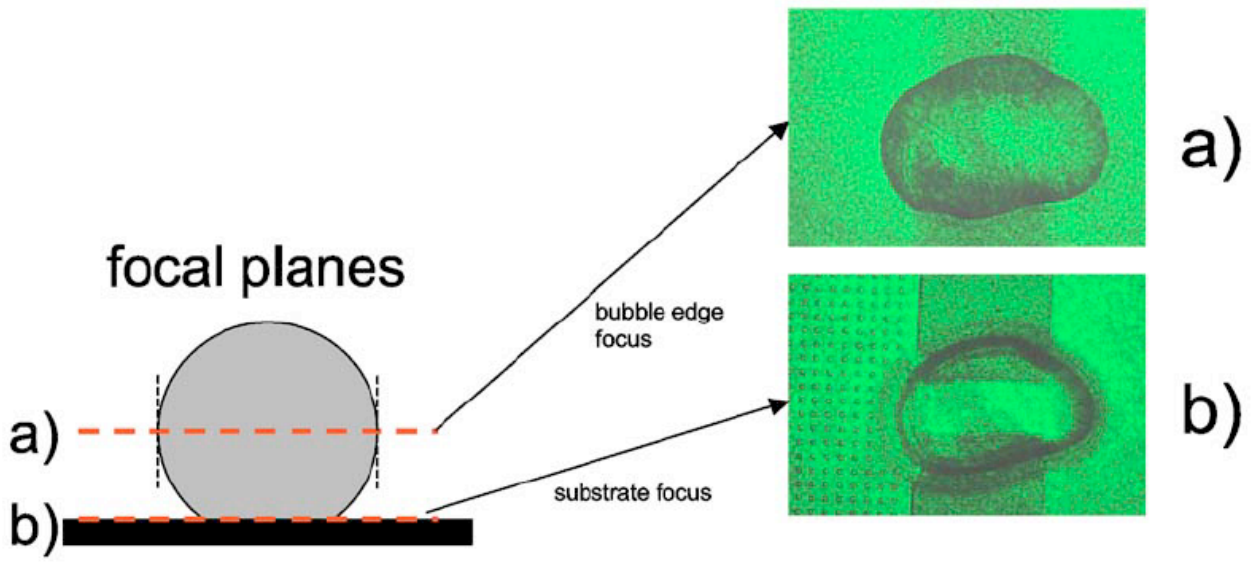


Figure 6

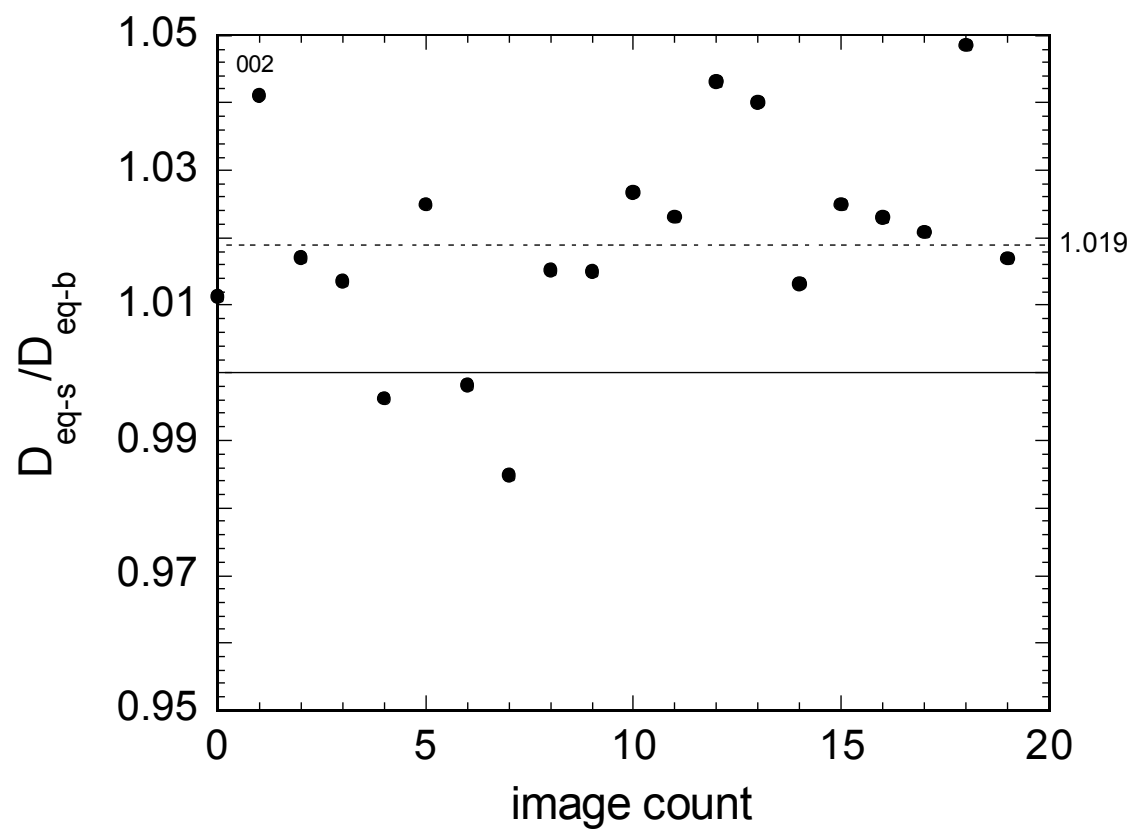


Figure 7

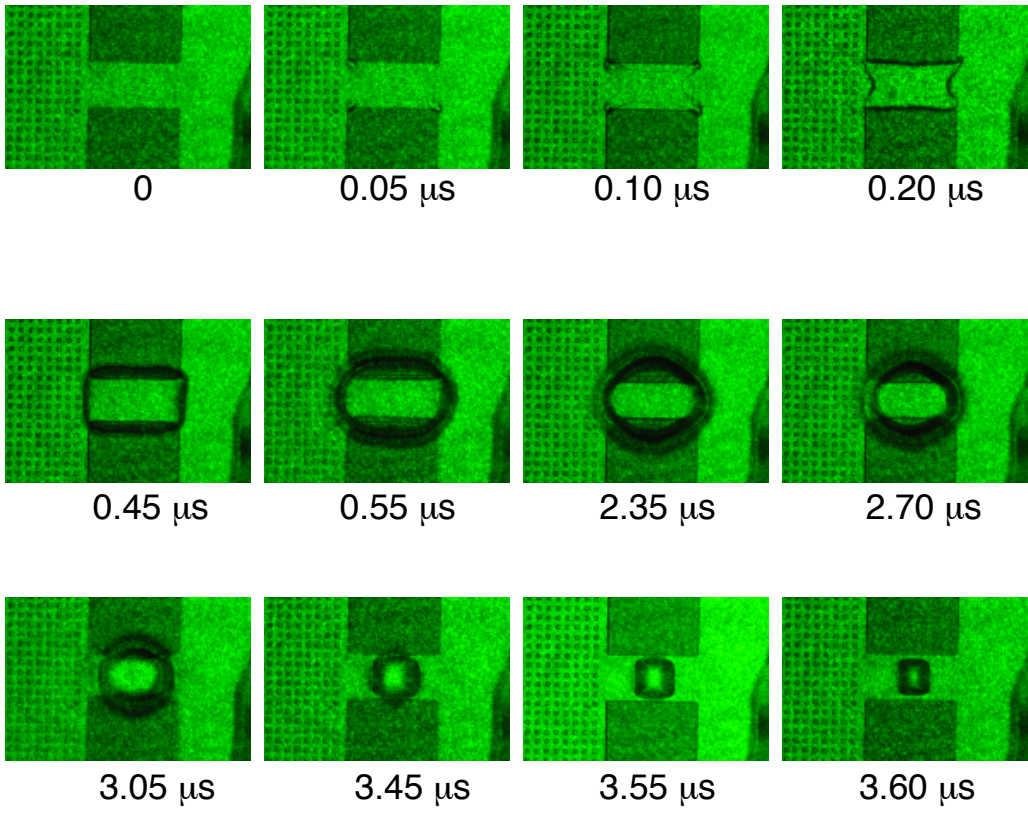
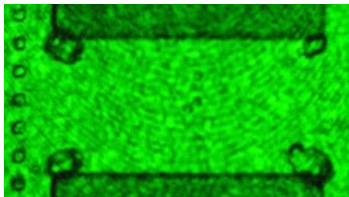
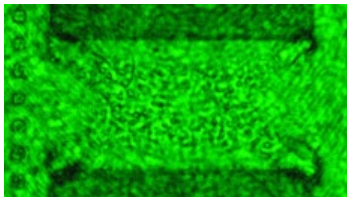


Figure 8

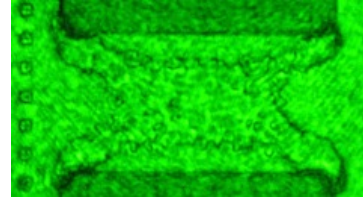
Img0016-1



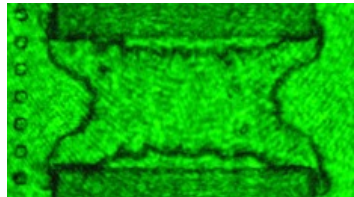
58 ns



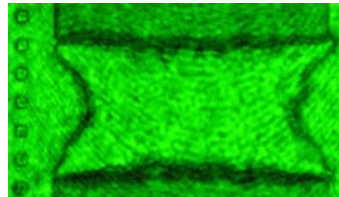
86 ns



142 ns



178 ns



246 ns

Figure 9

img0017: 7673,7687,7715,7733,7767

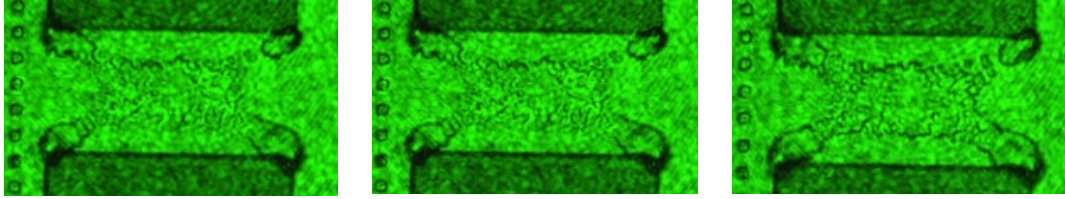


Figure 10